

Article

Enhancement of In Vitro Bioactivity of One-Step Spark Plasma Sintered Porous Titanium by Alkali-Treatment

Nan Lou ^{1,2}, Bin Zhu ^{1,2}, Lilin Luo ³, Yuqin Zhang ^{1,2,*} and Zengdong Meng ^{4,5,*}

¹ School of Materials Science & Engineering, Kunming University of Science and Technology, Kunming 650093, China

² National-Local Joint Engineering Laboratory for Technology of Advanced Metallic Solidification Forming and Equipment, Kunming 650093, China

³ Department of Orthopedic Pathology, The First People's Hospital of Yunnan Province, Kunming 650032, China

⁴ Department of Orthopedics, The First People's Hospital of Yunnan Province, Kunming 650032, China

⁵ Key Laboratory of Digital Orthopedics of Yunnan Province, Kunming 650032, China

* Correspondence: zyzkust@163.com (Y.Z.); menggu7119@vip.sina.com (Z.M.)

Abstract: Bioactivity and stress shielding are the most important problems of medical implanted porous titanium. In this study, porous titanium with 40% porosity was prepared by one-step spark plasma sintered (SPS) technology, and the surface of porous titanium was modified by a simplified alkali treatment method. The effects of a high concentration on pore properties, mechanical properties, and biological activities of porous titanium were investigated. The results show that the surface of porous titanium treated with a high concentration of alkali forms an interconnected network layer, which provides nucleation points for the formation of apatite. Porous titanium can still meet the requirements of hard tissue replacement after treatment with high-concentration alkali solution (yield strength (130 MPa) and elastic modulus (6.0 GPa)). A layer of apatite is formed on the surface of porous titanium after alkali treatment. The ability of inducing apatite formation increases with the increase of lye concentration. In addition, the results of proliferation and live dead cell staining of bone mesenchymal stem cells (BMSC) showed that alkali treatment had no toxic effect on the cells. With the increase of concentration, the cell activity was significantly enhanced. Therefore, the bioactive porous titanium modified with simplified alkali has a good medical prospect as artificial bone material.

Keywords: porous titanium; alkali-treatment; network structure; mechanical properties; in vitro bioactivity



Citation: Lou, N.; Zhu, B.; Luo, L.; Zhang, Y.; Meng, Z. Enhancement of In Vitro Bioactivity of One-Step Spark Plasma Sintered Porous Titanium by Alkali-Treatment. *Metals* **2022**, *12*, 2004. <https://doi.org/10.3390/met12122004>

Academic Editors: Irena Paulin and Crtomir Donik

Received: 18 October 2022

Accepted: 21 November 2022

Published: 23 November 2022

Publisher's Note: MDPI stays neutral with regard to jurisdictional claims in published maps and institutional affiliations.



Copyright: © 2022 by the authors. Licensee MDPI, Basel, Switzerland. This article is an open access article distributed under the terms and conditions of the Creative Commons Attribution (CC BY) license (<https://creativecommons.org/licenses/by/4.0/>).

1. Introduction

Titanium has been used as artificial bone materials under biomechanical load-bearing conditions because these substances have excellent mechanical properties and biocompatibility [1–4]. However, the elastic modulus of Ti (106.4 GPa) is quite different to that of human bone (2–30 GPa), resulting in a stress shielding effect at the implantation interface that eventually leads to undesirable side effects. Implementing porous Ti can reduce its elastic modulus significantly to improve mechanical fitness [5–7]. In recent years, Spark plasma sintering (SPS) has become the most effective sintering method for ceramics, metals, alloys, and composites because of its rapid densification and one-step molding [8,9]. Zhang et al. [10] successfully prepared porous titanium with a porosity of 38% by the one-step SPS technique using NH_4HCO_3 as a space holder without binder. Porous titanium not only has a large plasticity, but also has a suitable elastic modulus (11.2 GPa, close to the modulus of human bone) and a high compressive strength (287 MPa).

The introduction of porous structures favors the long penetration of tissue cells, even so, porous titanium is still a biologically inert material and cannot actively induce

phosphate deposition. As a result, it cannot promote chemical bonding between bone tissue and implants and its bone integration ability is poor, rendering limited clinical application. To address this issue, various surface modifications are applied to Ti and its alloys to improve their biological activity. At present, these modifications include plasma spraying, ion implantation, chemical deposition, and micro-arc oxidation technology, which enhance the bioactivity of Ti by changing the chemical composition, roughness, and morphology of its surface [11–17]. Among these methods, treatment with a strong alkali solution has been widely investigated because of its operational convenience, practicality, and effectiveness [18,19]. Yao et al. [20] used acid-alkali treatment to form micro-nanostructures on the surface of porous Ti samples, which effectively improved the bioactivity without damaging the elastic modulus and compressive strength. Zeng et al. [21] used alkali treatment to fabricate rough, homogeneous nano-reticular structures on Ti implant surfaces, and in vivo experiments in animals showed that these implants contributed to a sustained induction of osteogenesis and exhibited a faster osseointegration ability than conventional Ti implants. Improved osseointegration may be observed because the nanoscale surface presents a larger surface area that can better promote protein adsorption, cell adhesion and proliferation, gene regulation, and tissue integration [22,23]. In addition, nanostructures on Ti surfaces can also alter conformation of the arginine-glycine-aspartate-serine adhesion ligand to promote cell adhesion, and these ligands may be more exposed on nanoscale surfaces than on other types of surfaces [24]. Kim et al. [25] soaked commercial pure Ti plates and powder in 5 M NaOH and 5 M KOH solution for 24 h in the same temperature range (37–90 °C) and formed nanostructures of hydrated titanate layer on their surfaces, increasing the surface area by 50–220 times. However, in vitro cell culture experiments showed that KOH treatment or higher temperatures (60 °C or 90 °C) induced a decrease in cell adhesion and differentiation ability.

A large number of studies have shown that alkali treatment can significantly improve the bioactivity of titanium and titanium alloys [26–32]. However, there is little discussion on how different alkali concentrations affect the construction of surface nano-reticular layers, with resultant effects on the pore characteristics, mechanical properties, and biological activities of porous titanium. In this study, we aim to describe the resultant effects on pore characteristics, chemical composition, mechanical properties, mineralization, and in vitro bioactivity. To achieve this, we prepared porous titanium with 40% porosity by one-step SPS. In addition, the porous titanium was treated with 5 M, 10 M, and 15 M NaOH solutions at 60 °C for 24 h to prepare a nanoscale network of sodium titanate on its surface. The resultant surface pore characteristics, chemical composition, and mechanical properties are discussed; in vitro mineralization simulations are conducted, as well as cell viability tests.

2. Materials and Methods

2.1. Preparation of Materials

Figure 1 contains a flow chart illustrating the preparation of porous titanium and its subsequent alkali treatment. For raw materials, we used Ti powder (purity > 99.5%, particle size <30 µm, (Zhong Nuo Advanced Material Technology, Beijing, China), NH_4HCO_3 (AR-grade purity, Aladdin Biochemical Technology, Shanghai, China), and NaOH particles (purity > 99.5%, Feng Chuan Chemical Reagent, Tianjin, China). First, 15 g of blended Ti and NH_4HCO_3 powder (with a NH_4HCO_3 ratio of 40% vol) was weighed, pre-pressed, and the blank body was loaded into a graphite mold before sintering was conducted using spark plasma sintering equipment (SPS-515S, Syntex Inc., Kawasaki, Japan).

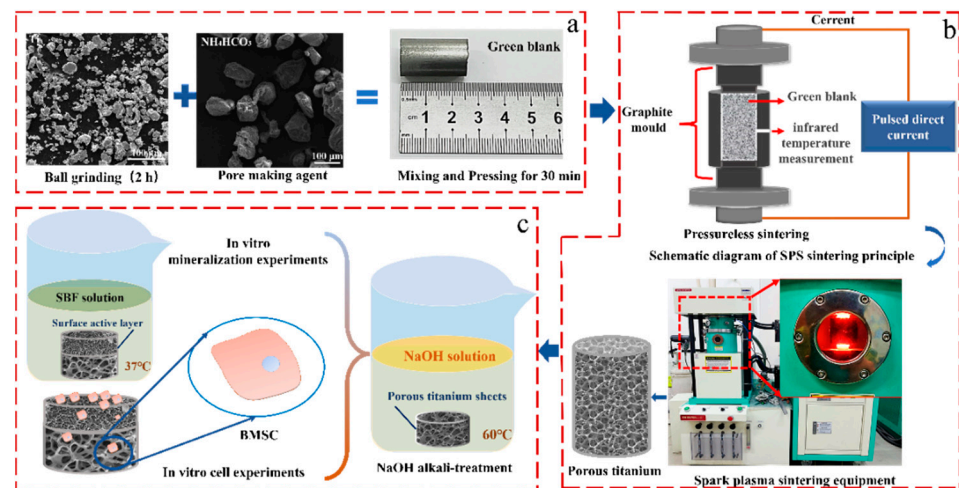


Figure 1. Experimental flow chart: (a) The Ti powder of ball milling for 2 h was mixed with NH_4HCO_3 , and the blank was pressed for 30 min. (b) The blank formed by pressing was put into the sintering chamber of SPS sintering equipment, and porous titanium was sintered in one step for 10 min. (c) Sintered porous titanium was cut into round pieces and soaked in a high concentration of sodium hydroxide solution for 24 h for alkali treatment modification. The immersion temperature was maintained at 60 °C using a constant water bath. Finally, in vitro biological activity evaluation of alkali-treated porous titanium was carried out (in vitro mineralization experiment and cell proliferation and live dead cell staining experiment of bone marrow stem cells).

2.2. Alkali Treatment

The pore structure of porous titanium was protected by non-pressure sintering. NaOH was prepared at concentrations of 5, 10, and 15 mol/L (M) (Table 1). Porous Ti samples produced by sintering were placed in respective NaOH solutions at 60 °C and soaked for 24 h. Thereafter, the Ti samples were removed, cleaned first ultrasonically and then with absolute ethanol and deionized water, and lastly dried in an electric blast drying at 40 °C for 2 h for later use.

Table 1. The preparation and use of different NaOH concentration.

Sample Number	NaOH Granules (g)	Deionized Water (mL)
1# (Untreated porous titanium)	0	0
2# (Porous titanium treated with 5 M NaOH)	10	50
3# (Porous titanium treated with 10 M NaOH)	20	50
4# (Porous titanium treated with 15 M NaOH)	30	50

2.3. Characterization

The surface morphology and composition of the samples were analyzed via scanning electron microscope (SEM) (Quanta 200, FEI, Waltham, MA, USA) and energy-dispersive spectrometer (EDS). An X-ray photoelectron spectrometer (XPS, Thermo Scientific Escalab 250Xi, Waltham, MA, USA) was used to analyze the valence and chemical composition of Ti surface elements. The Ti pore structure was observed with a metallographic microscope (Nikon ECLIPSE MA200, SHIMADZU, Tokyo, Japan), and pore parameters were analyzed by Image J software (version 1.51, National Institutes of Health, NIH, Bethesda, MD, USA). Following GB/T33820-2017 standards, the porous samples were cut into a cylinder with a diameter-to-height ratio of 1:2 and compression tests were performed on a microcomputer-controlled electronic universal testing machine (Criterion 40, MTS, Eden Prairie, MN, USA). The loading rate was 0.5 mm/min, and the average value of a group of samples was measured thrice.

2.4. In Vitro Bioactivity Experiment

Artificial simulated body fluid (SBF) of our own configuration was used for the mineralization experiment, and the components of the solution were as follows: NaCl 8.00 g, KCl 0.40 g, NaHCO₃ 0.35 g, CaCl₂ 0.14 g, MgSO₄·7H₂O 0.10 g, Na₂HPO₄·12H₂O 0.12 g, KH₂PO₄ 0.06 g, glucose 1 g, and 1 L deionized water, evenly stirred. The mineralization period was 14 days and the SBF solution was changed daily.

To investigate the effect of different alkaline concentrations on cellular activity, cell proliferation and viability experiments were conducted. Bone marrow mesenchymal stem cells (BMSC) (provided by the Institute of Primate Translation, Kunming University of Science and Technology, Kunming, China) were selected for culture and collected by trypsin digestion. The cells were resuspended in 1 mL high-glucose Dulbecco's modified Eagle's medium (α -MEM, Gibco, Gaithersburg, MD, USA) for cell counting. Cells were seeded into a 96-well plate (3×10^3 cells per well) and 100 μ L of sample extracts were added to the well plates according to experimental groups. Three wells containing blank controls (100 μ L high-glucose Dulbecco's modified Eagle's medium per well) were set at different time points, and CCK-8 (Sigma, Louis, MO, USA) was detected after 24 h, 48 h, and 72 h, respectively. The 96-well plate was removed, 10 μ L CCK-8 solution was added to each well, and then put back in the incubator to avoid light and incubated for 4 h. The optical density value of each well in the 96-well plate was detected by microplate reader at 450 nm.

The four Ti sample types (refer to Table 1) were sterilized by ultraviolet irradiation for 1 h and placed in 24-well plates. BMSC were seeded onto each sample surface at a density of 1×10^4 cells per well and incubated for 72 h in a CO₂ incubator. Thereafter, the medium was removed, samples were rinsed once with phosphate-buffered saline solution, and 500 μ L of calcein AM and propidium iodide stain (CA1630, Solarbio, Beijing, China) was added prior to another 20 min incubation period at 25 °C. The staining solution was sucked off, and the sample was rinsed once with phosphate-buffered saline solution. Lastly, the sample was placed on a slide under a cover glass and observed upside down under a laser confocal microscope (FV1000, Olympus, Tokyo, Japan).

2.5. Statistical Analysis

All statistical analyses were performed with SPSS software (version 16.0, SPSS Inc., Chicago, IL, USA). The results were expressed as the mean \pm standard deviation (SD), the independent experiment was duplicated at least three times. A one-way ANOVA was used to analyze the data. It was considered statistically significant when * $p < 0.05$.

3. Results

3.1. Pore Characteristics

Figure 2 shows the optical micromorphology and pore size frequency distribution of porous Ti across test groups, with pore size ranging from 50 μ m to 700 μ m. The porosity, pore size, and roundness of NaOH-treated porous Ti were analyzed using ImageJ software. As the concentration of NaOH solution increased, the porosity of Ti decreased from 40.97% to 39.57%, average diameter decreased from 215.2 μ m to 201 μ m, and hole roundness decreased from 0.629 to 0.552.

These results indicate that the concentration of NaOH used had little effect on the porosity and pore size, but significantly reduced the hole roundness of porous Ti. Pore size on the surface of untreated porous Ti was evenly distributed (Figure 2a). At NaOH treatment concentrations under 15 M, the number of pores between 50 μ m and 100 μ m decreased sharply due to the corrosive effect of the NaOH solution. As independent small pores became eroded, they expanded and connected with one another to form larger pores, which increased the pore connectivity to a certain extent. However, when the NaOH concentration reached 15 M, a large number of micropores (<50 μ m) appeared on the surface of the porous Ti (metallographic diagram in Figure 2d), which was due to a pitting corrosive effect that increased the number of independent micropores and reduced pore connectivity. Studies have shown that 100–500 μ m pore sizes are most suitable for tissue cell

adhesion and ingrowth, and the three-dimensional connected pore structure is conducive to the transport of blood and nutrients. Therefore, the alkaline concentration should not be too high during treatment to avoid a large number of independent micropores, which would affect the connectivity of the pores [33–36].

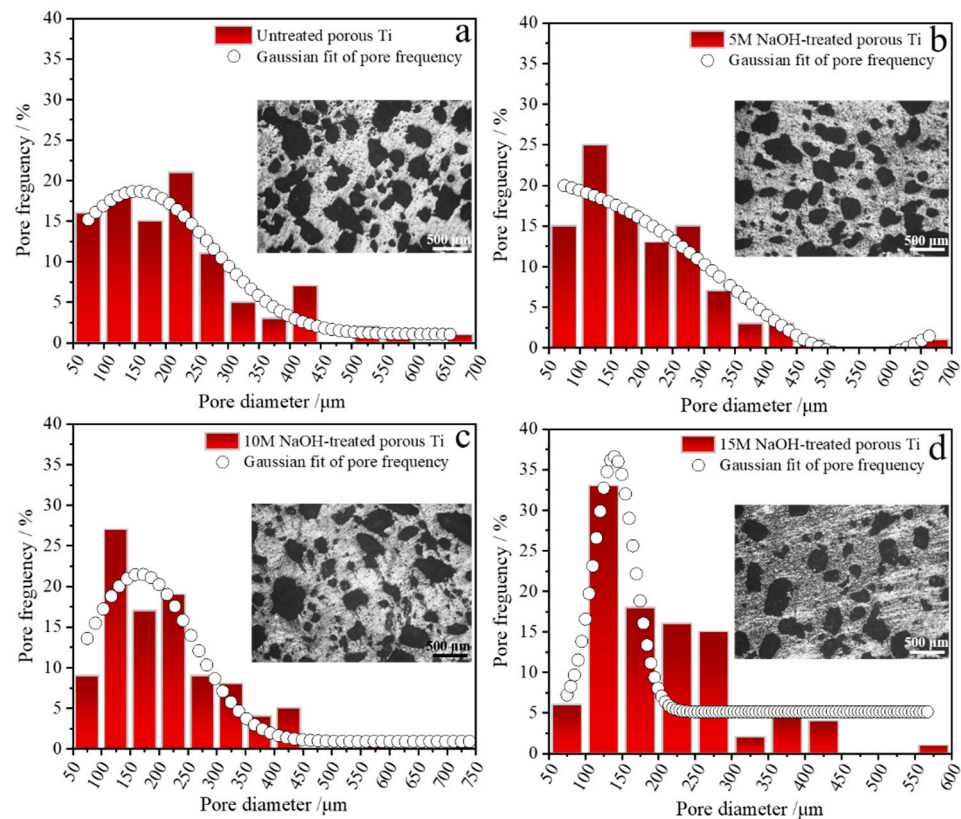


Figure 2. Optical microscopic morphology and aperture size frequency distribution of porous Ti after being treated with different concentrations of NaOH. (a) Untreated porous Ti. (b) 5 M NaOH-treated porous Ti. (c) 10 M NaOH-treated porous Ti. (d) 15 M NaOH-treated porous Ti.

3.2. Microstructure and XPS Analysis

Figure 3 shows the SEM morphology of porous Ti surfaces exposed to different concentrations of NaOH. The surface of untreated porous Ti was relatively smooth compared to the rough surfaces of samples that received alkali treatment and were covered with a layer of needle-like material. Local magnification of the yellow boxes in Figure 3 reveals that a layer of nanoscale reticular structures formed on the surface of porous Ti after NaOH treatment. At a concentration of 5 M NaOH (Figure 3b), these reticular structures were relatively independent with shallow pores. With an increase in NaOH concentration, a three-dimensional interconnected reticular structure took shape. At 10 M NaOH, the network structure was interwoven and uniform in thickness, pores were deepened, and a flower cluster-like nanostructure appeared (Figure 3c). When the concentration of NaOH treatment was 15 M (Figure 3d), the pores exhibited a larger diameter and deepened, representing a significant contrast in morphology. We conclude that an increase in NaOH solution concentration is conducive to the formation of a three-dimensional and interconnected nanonetwork structure on the surface of porous Ti, which increases its surface area and roughness.

Figure 4 shows the surface scan and EDS energy spectrum of a needle-like structure, and it shows the point scan and EDS energy spectrum of a flower cluster-like structure, as had been observed in Figure 3c. The needle-like material was mainly composed of Na and O elements with atomic percentages of 51.56% and 47.68%, respectively, and this Na:O atomic ratio of approximately 1:1 indicates that the needle-like material was residual

NaOH on the Ti surface. Point scanning of point A in Figure 4c shows that the structure is mainly composed of Na, Ti and O, with atomic percentages of 28.92%, 9.43% and 61.64%, respectively. We speculate that the substance may be sodium titanate salt. However, the changes in chemical composition and element content of porous Ti after varying NaOH treatments need to be further analyzed by XPS.

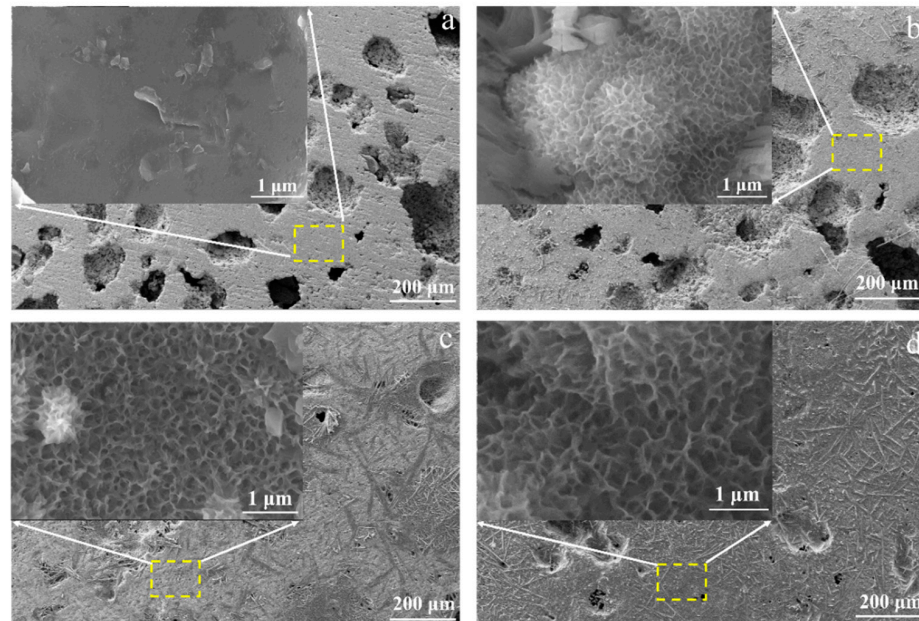


Figure 3. SEM morphologies of porous titanium treated with different concentrations of NaOH solutions: (a) Untreated porous Ti. (b) 5 M NaOH-treated porous Ti. (c) 10 M NaOH-treated porous Ti. (d) 15 M NaOH-treated porous Ti.

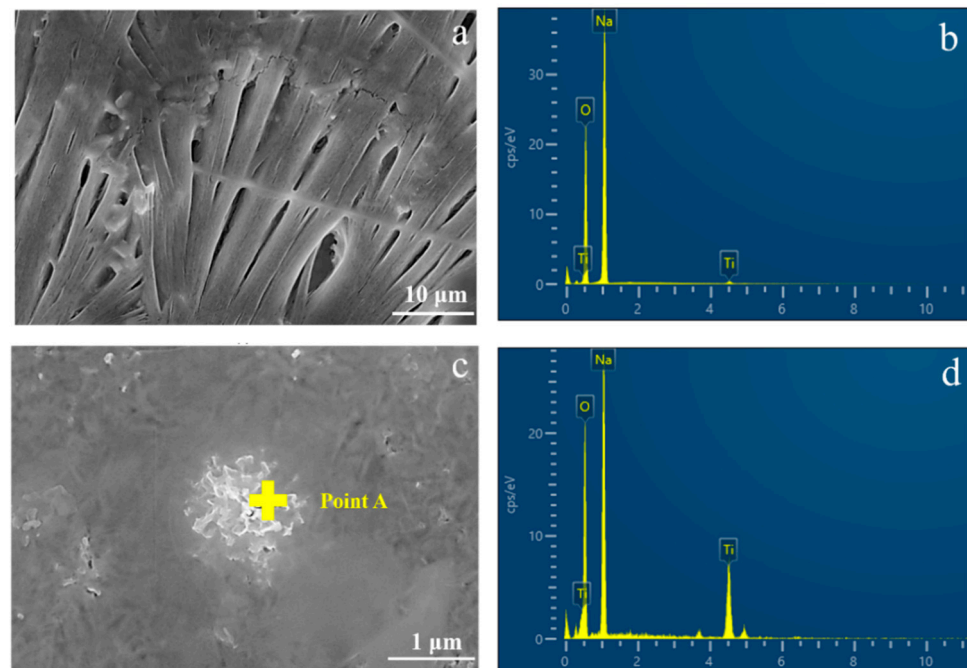


Figure 4. (a) Surface sweep of the needle-like structure observed in Figure 3c, along with (b) its EDS energy spectrum; (c) Point scan of the flower cluster-like structure observed in Figure 3c, along with (d) its EDS energy spectrum.

Figure 5 shows the full XPS spectrum of NaOH-treated Ti surfaces. The main components of untreated Ti surfaces were Ti, O, and C. After NaOH treatment, the porous Ti surface exhibited four elements: Ti, O, Na, and C. The carbon element may be from molecular pollution introduced by the diffusion pump oil of the test system itself or may be from carbon pollution from the air. O and Na may originate from sodium titanate, the chemical product of alkaline-treated Ti surfaces. Ti exposed to air forms a passivation film (TiO_2) on its surface and, after soaking in NaOH, a layer of sodium titanate will be generated on its surface according to the following reaction [37–39]:

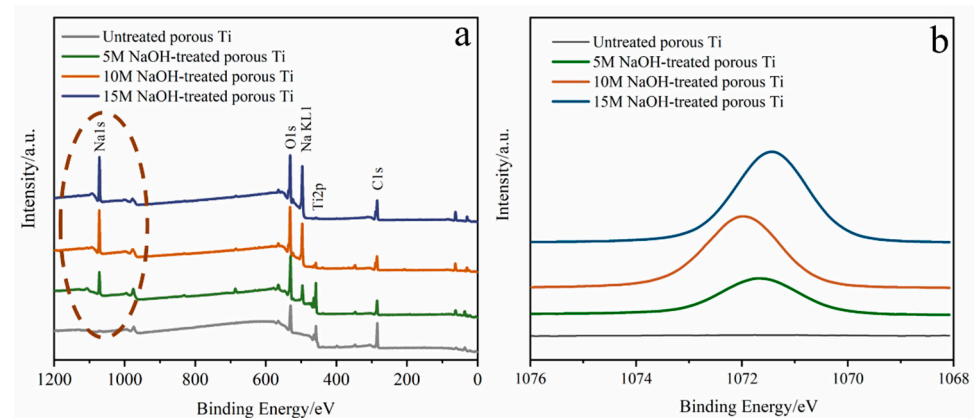
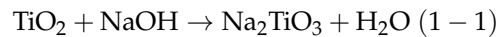


Figure 5. (a) XPS full spectrum of porous Ti treated with different NaOH concentrations and (b) the high-resolution fine spectrum of Na1s, as circled with brown dashes in (a).

The binding energies of Na^+ on the surface of Ti treated with 5 M, 10 M, or 15 M NaOH were 1071.67 eV, 1071.97 eV, and 1071.41 eV, respectively, which correspond to the binding energies of Na^+ in Na_2TiO_3 and Na_2CO_3 as shown in Figure 5b.

Figure 6 shows the high-resolution fine peak-fitting diagram of the binding energy of O element on porous Ti following its treatment with different concentrations of NaOH. By correcting for the standard peak of C1s at 284.8 eV, it was found that the binding energy of O ranged from 529.87 eV to 530.98 eV, which corresponds with the binding energy of O^{2-} in metal oxides. In the fine spectrum of untreated porous titanium O1s and the porous titanium O1s treated with 5 M NaOH, the respective binding energies at 531.50 eV and 531.86 eV corresponded to that of O in the adsorbed water on the porous titanium surface (Figure 6a,b). The binding energy ranges from 531.50 eV to 531.60 eV, which corresponds with the appearance of O^{2-} in the metal carbonate after alkali treatment, the metal carbonate is mainly present due to the reaction of the residual on the porous titanium surface after high concentration treatment with CO_2 in the air to form Na_2CO_3 .

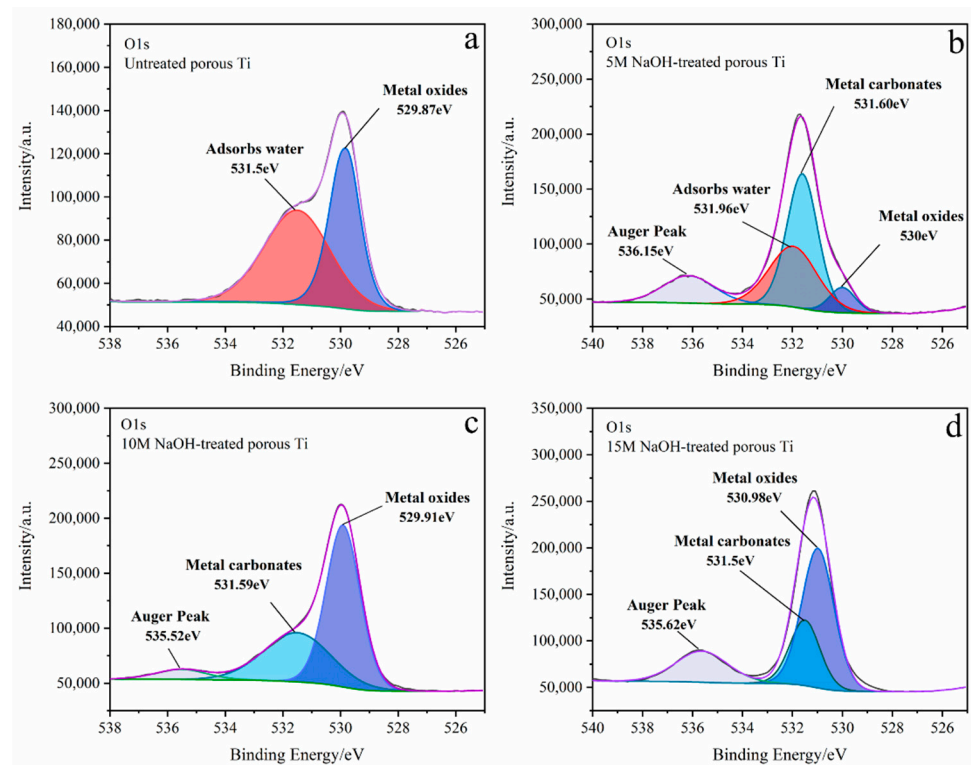


Figure 6. The high resolution fine peak fitting diagram of the binding energy of O element on porous Ti after NaOH treatment with different concentrations, (a) O1s peak fitting diagram of untreated porous Ti. (b) O1s peak fitting diagram of 5 M NaOH-treated porous Ti. (c) O1s peak fitting diagram of 10 M NaOH-treated porous Ti. (d) O1s peak fitting diagram of 15 M NaOH-treated porous Ti.

Figure 7 shows the high-resolution fine-peak fitting of Ti2p after alkaline treatment with different concentrations of NaOH. In the map for untreated Ti2p, the main peaks of Ti2p_{3/2} and Ti2p_{1/2} were at 458.8 eV and 464.5 eV, respectively, and the difference in binding energies between these peaks was 5.7 eV, which is consistent with the standard energy spacing of Ti metal oxides [40,41]. The relative contents of Ti and O were calculated via their relative sensitivity factors. The percentages of Ti and O atoms in untreated porous Ti were 17.62% and 38.93%, respectively, representing a ratio of approximately 1:2. Ti⁴⁺ exists on the surface of untreated porous Ti in the form of TiO₂, Ti⁴⁺ exists in the form of TiO₂ on the surface of untreated porous titanium, while Ti₂O₃ and TiO on the surface may be caused by incomplete oxidation of porous titanium in air after sintering, as shown in Figure 7a. The peak fitting of Ti2p after alkali treatment is shown in Figure 7b–d. The binding energies of the new double peaks are 459.03 eV and 464.73 eV (Figure 6b) after 5 M NaOH treatment, 458.34 eV and 464.04 eV (Figure 7c) after 10 M NaOH treatment, and 458.33 eV and 464.07 eV (Figure 7d) after 15 M NaOH treatment. The binding energy spacing is still 5.7 eV, which is consistent with the binding energy spacing of titanium metal oxides. For 5 M, 10 M, and 15 M NaOH treatment, the percentage of Ti atoms was 16.25%, 17.96%, and 18.85%, respectively, and the percentage of O atoms was 48.58%, 55.85%, and 54.32%, respectively. The ratio of Ti and O atoms is between 2.99–3.11, which is consistent with the ratio of Ti and O atoms in sodium titanate Na₂TiO₃. According to XPS semi-quantitative analysis, the content of Ti2p in Na₂TiO₃ increased from 39.12% to 66.79% with the increase in treatment concentration. The surface material composition of porous Ti following alkaline treatment is mainly TiO₂ and Na₂TiO₃ (in addition to the Ti matrix). Na₂TiO₃ content increased while that of TiO₂ decreased with an increase in NaOH treatment concentration. It was difficult to detect Ti in the matrix following exposure to a high concentration of NaOH (Figure 7c,d).

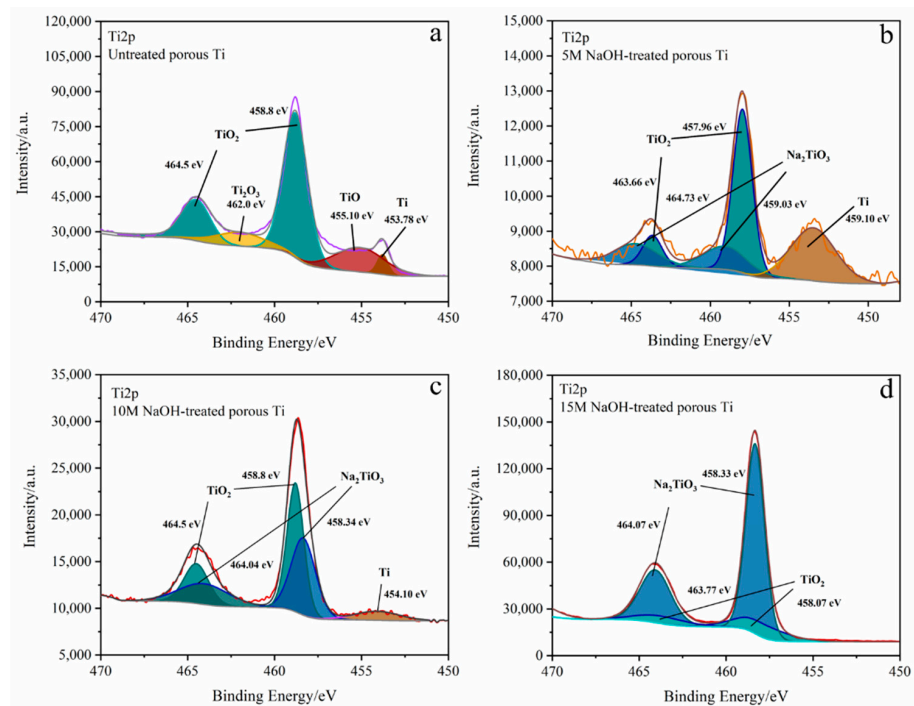


Figure 7. The high-resolution fine-peak fitting of Ti2p after alkaline treatment with different concentrations of NaOH, (a) Ti2p peak fitting diagram of untreated porous Ti. (b) Ti2p peak fitting diagram of 5 M NaOH-treated porous Ti. (c) Ti2p peak fitting diagram of 10 M NaOH-treated porous Ti. (d) Ti2p peak fitting diagram of 15 M NaOH-treated porous Ti.

3.3. Mechanical Property

Figure 8a is the compressive stress–strain curve of NaOH-treated porous Ti, and Figure 8b is the yield strength and elastic modulus of the synthesis. From the diagram, it can be seen that the compressive stress–strain curve deformation of the four porous titanium materials is divided into three stages: (I) elastic stage, (II) plastic stage, (III) densification stage. It is generally believed that the boundary between the elastic stage and the plastic stage is the yield limit. In the elastic stage, the stress–strain curve of porous titanium is basically linear. In the plastic stage, the stress slows down with the increase of strain, and a short plastic yield platform appears. Compaction occurs at the end of the plastic stage. As long as the porous structure collapses, the pressure decreases at this stage. When the collapsed hole walls are gradually compacted together, the required pressure rises again, so the final pressure curve shows an upward trend. The compressive stress–strain curves of porous titanium treated with different concentrations of alkali have a long yield deformation stage, which is similar to that of untreated porous titanium, indicating that the increase of alkali concentration will not destroy the plasticity and toughness of porous titanium. Furthermore, alkaline treatment decreased the yield strength of porous Ti from 168 MPa to 130 MPa and decreased the elastic modulus from 7.8 GPa to 6.0 GPa. In other words, NaOH treatment can significantly reduce the maximum bearing force and elastic modulus of porous Ti to effect permanent deformation. There were no significant differences in either the yield strength or elastic modulus of Ti between groups treated with 10 M and 15 M NaOH.

According to the literature [42–44], the shape and number of pores can significantly influence the performance of porous material under compression. When pores are sub-bicircular, pressure causes stress concentration at the pore tips, and stress overload near the hole can cause micro cracks. Due to the combined presence of micro cracks and stress concentration, stress continues to the load and the cracks extend rapidly. In other words, when the concentration of NaOH treatment was increased in our study, the roundness of Ti pores decreased, the number of pore tip increased, and as a result, the porous titanium became

prone to deformation under force. When the concentration is 15 M, the elastic modulus of porous titanium decreases while ensuring a certain compressive strength (130 MPa), which improves the mechanical fitness of porous titanium.

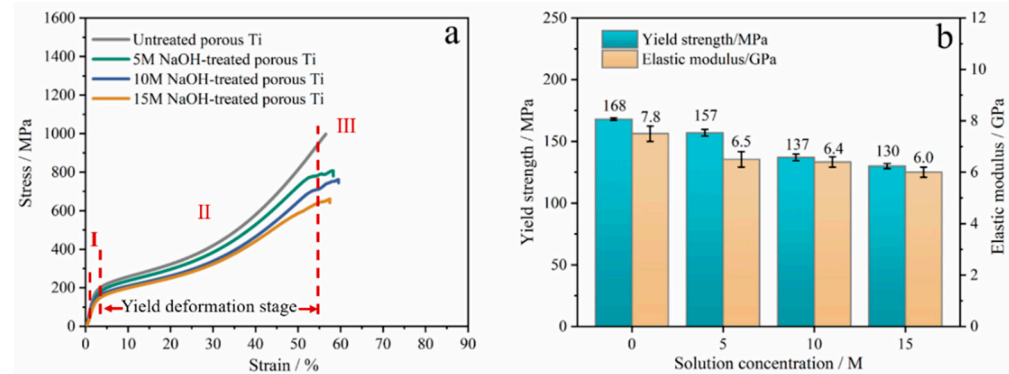


Figure 8. Compressive stress–strain curves, yield strength, and elastic modulus statistics of porous titanium treated with different concentrations of NaOH solution. (a) Compressive stress–strain curves of porous titanium treated with different concentrations of NaOH, (b) Compressive yield strength and elastic modulus histogram of porous titanium treated with different concentrations of NaOH.

3.4. In Vitro Bioactivity Evaluation

Figure 9 shows the surface morphology and sweep of porous Ti that had mineralized for 14 days after being treated with different concentrations of NaOH. Almost no mineralization occurred on the surface of untreated porous Ti, while uniformly distributed white flocculent material was deposited on NaOH-treated samples. At a 5 M concentration of NaOH, titanium was still visible in the matrix. As the NaOH concentration increased, the amount of sediment increased significantly until the porous Ti surface was almost completely covered at NaOH concentrations of 10 M and 15 M. Magnification of the flocculent sediment reveals that the porous network structure on the Ti surface was still distinctly visible after alkaline treatment. When the NaOH concentration was 10 M and 15 M, the sediment had entirely filled the pores of the network structure, and the cut distribution was uniform. Scans of the surface indicated that it was virtually covered by a uniform distribution of Ca, P, and O elements (Figure 9f,h).

Table 2 shows the proportions of elements present on the Ti surfaces of test samples after 14 days of mineralization. Untreated Ti possessed only trace elements of Ca and P. With the increase in NaOH concentration of treatments, the Ca, P, and O content on the Ti surface following mineralization increased significantly. The ratios of Ca to P atoms were 0.5, 1.62, 1.69, and 1.76 for NaOH concentrations of 0 M, 5 M, 10 M, and 15 M, respectively. The three ratios observed for NaOH-treated and mineralized Ti were close to the Ca:P ratio of apatite (1.67), and the samples of groups 3# and 4# contained relatively more elements after mineralization. In other words, when the concentration of NaOH treatment solution was 10 M and 15 M, the mineralization results of porous Ti are similar, and when the concentration was 10 M, the Ca:P following Ti mineralization was the closest to that of bone-like apatite.

Table 2. The proportions of elements present on the Ti surfaces of test samples after 14 days of mineralization.

Sample Number	Proportions of Elements (at%)				
	Ti	O	Ca	P	Na
1#	61.32	35.71	0.29	0.58	1.23
2#	14.65	59.22	11.09	7.05	2.25
3#	1.47	60.71	22.52	13.30	0.66
4#	1.92	61.33	22.05	12.56	0.69

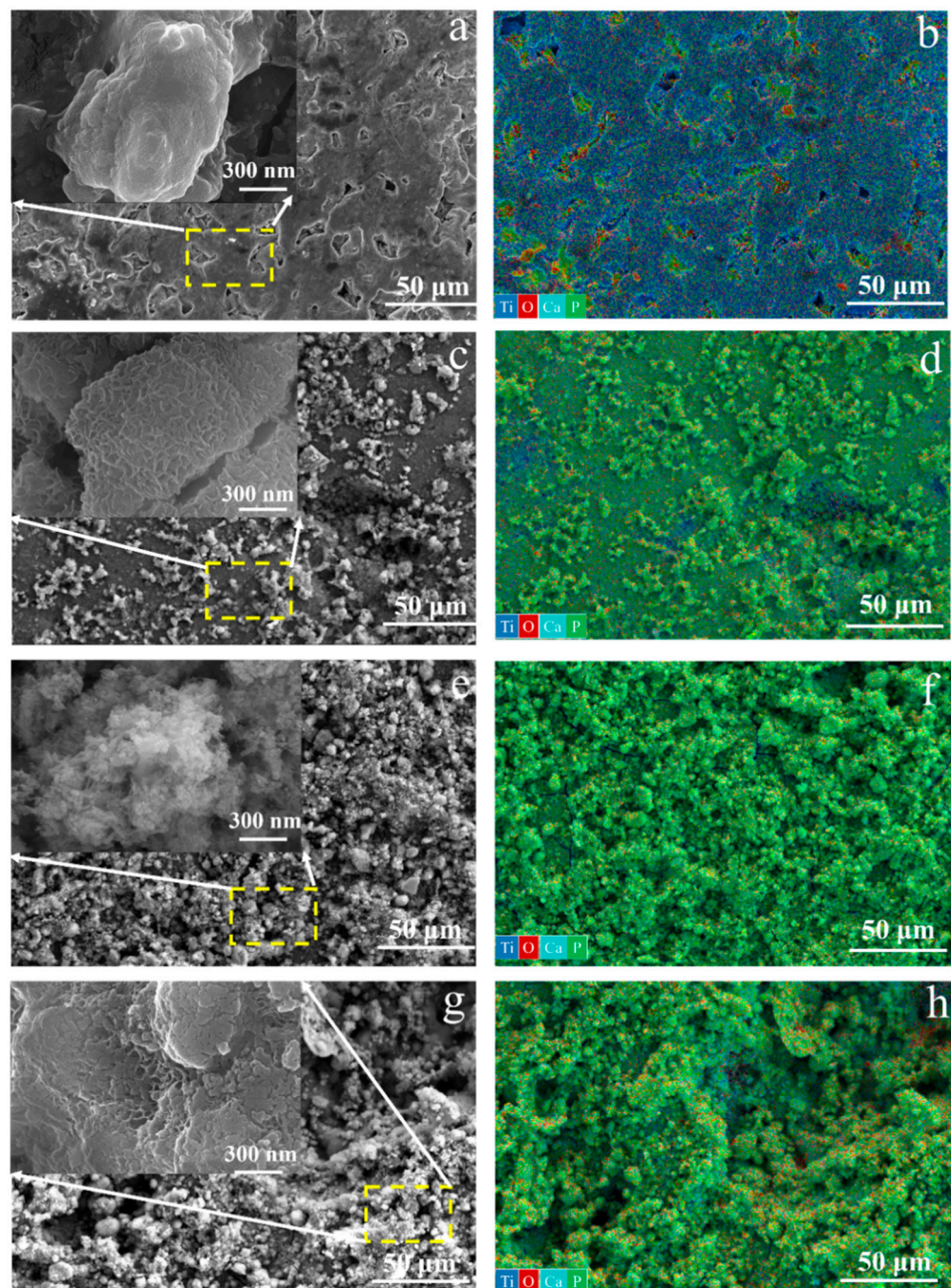


Figure 9. The surface morphology of porous titanium mineralized for 14 days after different concentrations of NaOH treatment. (a) Untreated porous Ti, (b) EDS diagram of untreated porous Ti, (c) 5 M NaOH-treated porous Ti, (d) EDS diagram of 5 M NaOH-treated porous Ti, (e) 10 M NaOH-treated porous Ti, (f) EDS diagram of 10 M NaOH-treated porous Ti, (g) 15 M NaOH-treated porous Ti, (h) EDS diagram of 15 M NaOH-treated porous Ti.

Figure 10 illustrates the mineralization mechanism observed. The deposition of alkali-treated titanium surface apatite when immersed in SBF can be explained by electrostatic attraction principles. Ion exchange occurs between Na^+ in the sodium titanate on the porous titanium surface behind the base, and H_3O^+ in the SBF. This leads to the formation of many negatively charged Ti-OH functional groups on the Ti surface; Ca^{2+} with the negatively charged Ti-OH attracts to aggregate on the porous titanium Ti surface due to electrostatic attraction. These Ti OH-functional groups are able to induce apatite nucleation. Due to the negative charge of Ti-OH [45], it attracts the positively charged Ca^{2+} to the Ti

surface. As Ca^{2+} accumulates, it binds to the negatively charged PO_4^{3-} and CO_3^{2-} to form a calcium phosphate, which is eventually converted to apatite. Once the apatite is nucleated, it will continue to grow by absorbing both Ca^{2+} and PO_4^{3-} , eventually forming a dense and uniform apatite coating. The results showed that the higher the lye concentration, the thicker the sodium titanate mesh layer was, and the more Na^+ was released, enhancing the ability to induce apatite formation. When treated with 10 M and 15 M NaOH, porous Ti showed an excellent ability to induce the formation of bone-like apatite, significantly improving its potential for bioactivity.

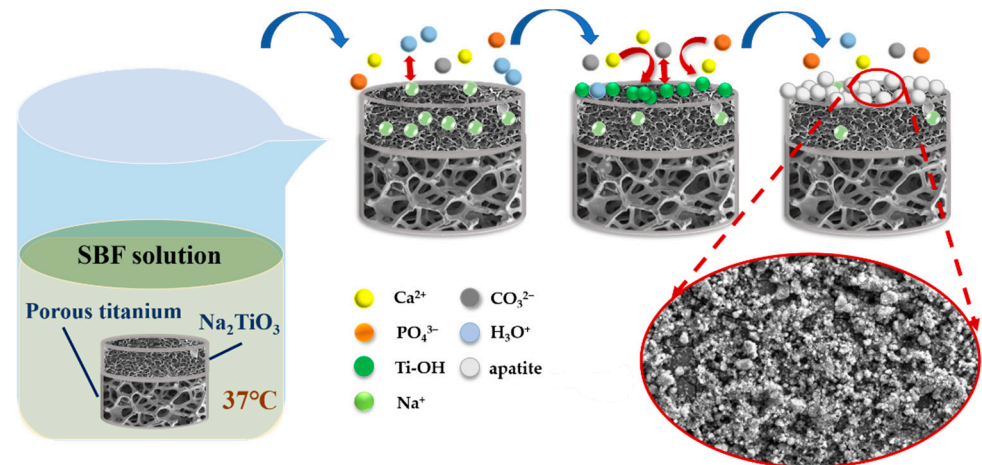


Figure 10. Schematic diagram of the mineralization mechanism of porous Ti treated with NaOH.

Figure 11 outlines the cell proliferation assay for BMSCs with porous titanium treated with different concentrations of base. Mitochondria in living cells oxidize and reduce the dehydrogenase in cck-8 to form a water-soluble orange-yellow formazan dye, while dead cells do not have this function. The optical density (OD) of formazan was measured by a microplate reader at a wavelength of 450 nm, that is, the absorbance of a substance at a specific wavelength. The absorbance is proportional to the concentration of the substance, so the larger the OD value, the more the number of living cells. At the early stage of BMSC proliferation (24 h), there was no significant difference in cell proliferation between the test and control groups ($* p > 0.05$). However, the OD values of the four test materials gradually increased over time. After 48 h of culture, BMSC activity was significantly enhanced on the porous Ti surfaces that had been subjected to NaOH treatment; the optical density value of the cells increased with an increase in NaOH concentration. When the concentration of NaOH was 15 M, the cell proliferation on the Ti surface was significantly higher than that of cells on Ti treated with 10 M and 5 M NaOH ($* p < 0.05$), which was statistically significant. After 72 h of culture, the effect of NaOH-treated porous Ti on cell proliferation was significantly stronger than that of untreated porous Ti. At this stage, the results of the cell proliferation experiment in the control group were consistent with that of the cell dead cell staining experiment. We can thus conclude that alkaline treatment had no toxic effect on cells and significantly improved the activity of porous titanium, where the increased concentration of sodium hydroxide treatment is favorable to cell proliferation.

Figure 12 shows the Calcein-AM and propidium iodide staining results of BMSC cultured on different titanium substrates for 3 days. The blue stains are cell nuclei, green-stained cells are living cells, and red-stained cells are dead. After 72 h of BMSC culture, a small number of dead cells appeared in the blank control group and on untreated Ti surfaces, but there were still many green living cells on the porous surface, showing good activity. The cells of all NaOH-treated groups were in good condition. Compared to the untreated group, NaOH-treated groups displayed a significant increase in the number of green viable cells and only a few red dead cells. This is because the three-dimensional interconnected nanoscale network structure on the surface of NaOH-treated Ti is conducive

to the growth and attachment of cells. Compared to the blank control group, the 10 M and 15 M NaOH-treated groups displayed a similar number of living cells but less dead cells. The results indicate that porous Ti promotes cell proliferation effectively and increase cell activity following treatment with high concentrations of NaOH.

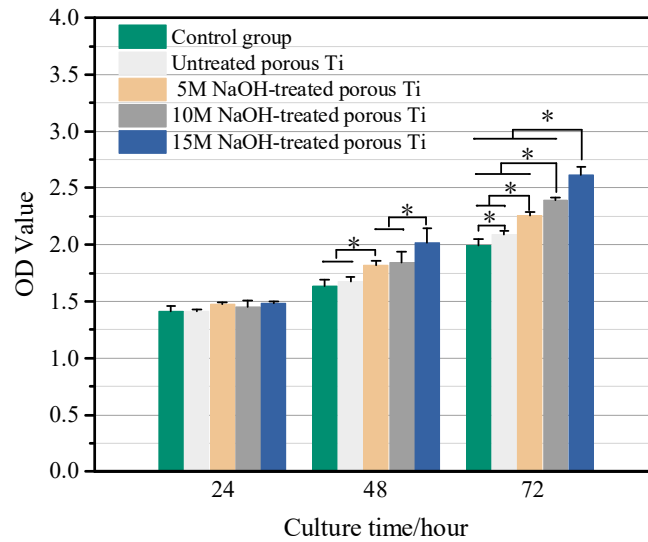


Figure 11. Proliferation of BMSC on different porous titanium surfaces, * $p < 0.05$, $n = 3$.

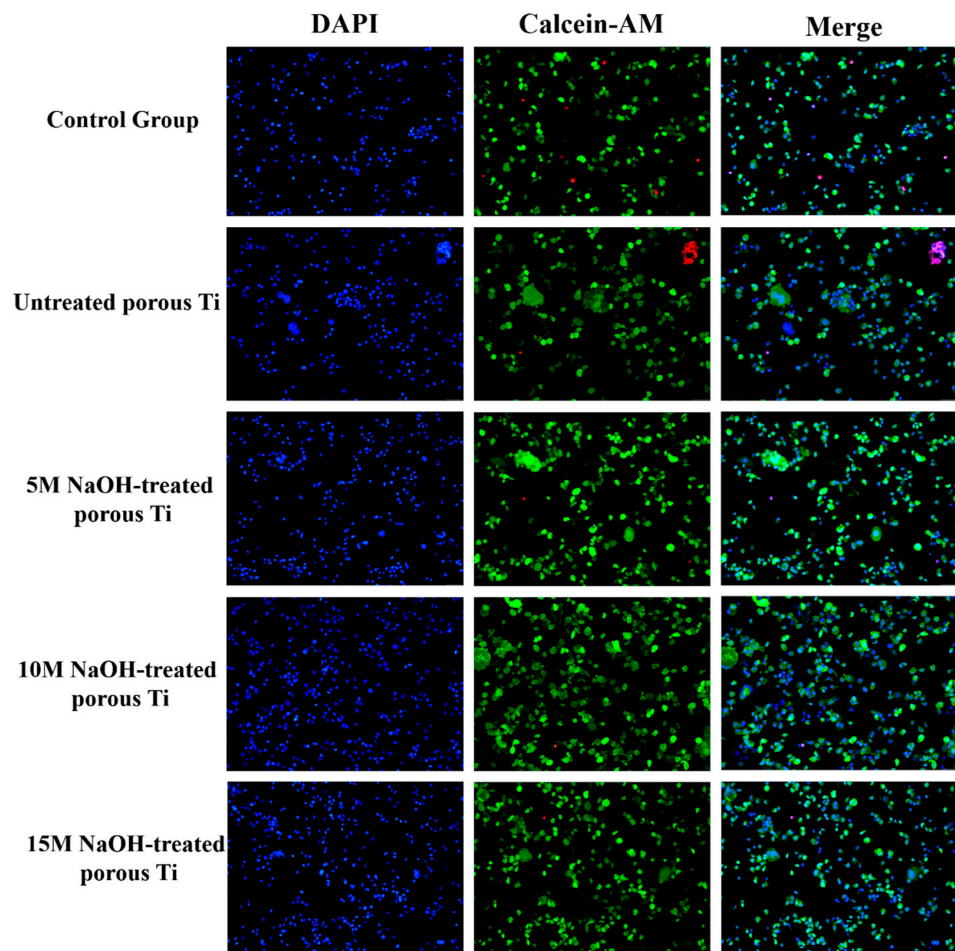


Figure 12. Live and dead cell staining of BMSC on different porous Ti surfaces. Blue stains are cell nuclei, green cells are live cells, and red cells are dead.

4. Conclusions

A porous titanium surface prepared using the SPS one-step forming method was rapidly bioactivated by alkali treatment. Compared with those of untreated porous titanium, the surface activity, surface area, and roughness of porous titanium were significantly enhanced by the network structure prepared by alkali treatment. With the increase of alkali treatment concentration, the connectivity of the sodium titanate network on the porous titanium surface was better. The mechanical properties of porous titanium were not damaged by alkali treatment. The surface of the treated samples was mainly composed of sodium titanate and TiO₂. With the increase in the concentration of alkali treatment, the ability of porous titanium to induce apatite formation was enhanced. The number, survival rate, and cell activity of porous titanium BMSCs increased after alkali treatment. Therefore, in this study, the alkali treatment modification of low-modulus porous titanium prepared by the SPS one-step molding process not only improved its mechanical compatibility without destroying its plasticity and toughness, but also significantly enhanced the bioactivity of porous titanium in vitro. The alkaline treatment method in this study solves the problem of insufficient biological activity of medical titanium with low cost and high efficiency, which makes it have a potential application prospect in the biomedical field.

Author Contributions: Conceptualization, Y.Z. and Z.M.; methodology, N.L.; software, N.L.; validation, N.L., B.Z. and L.L.; formal analysis, N.L.; investigation, B.Z.; resources, N.L.; data curation, N.L.; writing—original draft preparation, N.L.; writing—review and editing, Y.Z. and Z.M.; visualization, N.L.; supervision, B.Z.; project administration, Z.M.; funding acquisition, Y.Z. All authors have read and agreed to the published version of the manuscript.

Funding: This research was funded by the Yunnan Major Scientific and Technological Projects (grant No. 202202AG050007), Key Projects of Basic Research Program of Yunnan Province (2019FA029), High-Level Medical Leading Talent Project of Yunnan Province (L-2018004), National Natural Science Foundation of China (31660262).

Institutional Review Board Statement: Not applicable.

Informed Consent Statement: Not applicable.

Data Availability Statement: Not applicable.

Conflicts of Interest: The authors declare no conflict of interest.

References

1. Annur, D.; Kartika, I.; Supriadi, S.; Suharno, B. Titanium and titanium based alloy prepared by spark plasma sintering method for biomedical implant applications—a review. *Mater. Res. Express* **2021**, *8*, 012001. [[CrossRef](#)]
2. Mour, M.; Das, D.; Winkler, T.; Hoenig, E.; Mielke, G.; Morlock, M.M.; Schilling, A.F. Advances in Porous Biomaterials for Dental and Orthopaedic Applications. *Materials* **2010**, *3*, 2947–2974. [[CrossRef](#)]
3. Zhang, X.P.; Yu, S.R.; He, Z.M. The present status of study of Ti alloy for dentistry. *Rare Met. Mater. Eng.* **2004**, *33*, 1243–1247.
4. Zhu, K.P.; Zhu, J.W.; Qu, H.L. Development and Application of Biomedical Ti Alloys Abroad. *Rare Met. Mater. Eng.* **2012**, *41*, 2058–2063.
5. Hao, D.; Lei, Z.; Yuqin, Z.; Zongyu, Z.; Fei, H. The microstructure, mechanical properties and in-vitro biological compatibility of porous Ti-40Nb alloy fabricated by spark plasma sintering. *Mater. Res. Express* **2019**, *6*, 1065f3. [[CrossRef](#)]
6. Li, F.; Li, J.; Xu, G.; Liu, G.; Kou, H.; Zhou, L. Fabrication, pore structure and compressive behavior of anisotropic porous titanium for human trabecular bone implant applications. *J. Mech. Behav. Biomed. Mater.* **2015**, *46*, 104–114. [[CrossRef](#)]
7. Hybasek, V.; Fojt, J.; Malek, J.; Jablonska, E.; Pruchova, E.; Joska, L.; Ruml, T. Mechanical properties, corrosion behaviour and biocompatibility of TiNbTaSn for dentistry. *Mater. Res. Express* **2020**, *7*, 015403. [[CrossRef](#)]
8. Alhazaa, A.; Assaifan, A.; Hezam, M.; Shar, M.A.; Umeda, J.; Kondoh, K. Effect of sintering temperature on the microstructure and mechanical properties of the Ti-2.5Zr alloy. *Mater. Res. Express* **2021**, *8*, 016522. [[CrossRef](#)]
9. Du, P.; Li, K.; Zhu, B.; Xiang, T.; Xie, G.Q. Development of non-toxic low-cost bioactive porous Ti-Fe-Si bulk metallic glass with bone-like mechanical properties for orthopedic implants. *J. Mater. Res. Technol.-JMRT* **2022**, *17*, 1319–1329. [[CrossRef](#)]
10. Zhang, L.; Zhang, Y.Q.; Jiang, Y.H.; Zhou, R. Mechanical behaviors of porous Ti with high porosity and large pore size prepared by one-step spark plasma sintering technique. *Vacuum* **2015**, *122*, 187–194. [[CrossRef](#)]
11. Yan, J.; Cao, C.; Dong, Y. Methods and efficacy of surface bioactivity modification for titanium and titanium alloy. *J. Clin. Rehabil. Tissue Eng. Res.* **2011**, *15*, 3921–3924.

12. Dai, J.J.; Zhu, J.Y.; Chen, C.Z.; Weng, F. High temperature oxidation behavior and research status of modifications on improving high temperature oxidation resistance of titanium alloys and titanium aluminides: A review. *J. Alloys Compd.* **2016**, *685*, 784–798. [[CrossRef](#)]
13. Jin, H. Research Status of Biomedical Titanium Alloys and Its Surface Modification. *Chin. J. Rare Met.* **2003**, *27*, 794–798.
14. Li, Y.; Li, C. Titanium implants: Strategies on surface modification and effect on osseointegration. *Chin. J. Tissue Eng. Res.* **2013**, *17*, 5395–5402.
15. Natu, V.; Pai, R.; Sokol, M.; Carey, M.; Kalra, V.; Barsoum, M.W. 2D Ti₃C₂T_z MXene Synthesized by Water-free Etching of Ti₃AlC₂ in Polar Organic Solvents. *Chem* **2020**, *6*, 616–630. [[CrossRef](#)]
16. Kobatake, R.; Doi, K.; Oki, Y.; Umehara, H.; Kawano, H.; Kubo, T.; Tsuga, K. Investigation of Effective Modification Treatments for Titanium Membranes. *Appl. Sci.* **2017**, *7*, 1022. [[CrossRef](#)]
17. Komasa, S.; Su, Y.M.; Taguchi, Y.; Yamawaki, I.; Tsutsumi, Y.; Kusumoto, T.; Nishizaki, H.; Miyake, T.; Umeda, M.; Tanaka, M.; et al. Bioactivity of Titanium Surface Nanostructures Following Chemical Processing and Heat Treatment. *J. Hard Tissue Biol.* **2015**, *24*, 257–265. [[CrossRef](#)]
18. Lu, C.F.; Huang, H.M.; Chu, C.H.; Li, W.L.; Hong, T.F. The Effects of Heat Treatment Atmosphere on the Bone-Like Apatite Inducement on the Alkali Treated Ti-6Al-4V Surfaces. *Procedia Eng.* **2012**, *36*, 179–185. [[CrossRef](#)]
19. Zhou, Y.; Wang, Y.B.; Zhang, E.W.; Cheng, Y.; Xiong, X.L.; Zheng, Y.F.; Wei, S.C. Alkali-heat treatment of a low modulus biomedical Ti-27Nb alloy. *Biomed. Mater.* **2009**, *4*, 044108. [[CrossRef](#)]
20. Yao, Y.T.; Liu, S.; Swain, M.V.; Zhang, X.P.; Zhao, K.; Jian, Y.T. Effects of acid-alkali treatment on bioactivity and osteoinduction of porous titanium: An in vitro study. *Mater. Sci. Eng. C-Mater. Biol. Appl.* **2019**, *94*, 200–210. [[CrossRef](#)]
21. Zeng, Y.H.; Yang, Y.Y.; Chen, L.Y.; Yin, D.R.; Zhang, H.H.; Tashiro, Y.; Inui, S.; Kusumoto, T.; Nishizaki, H.; Sekino, T.; et al. Optimized Surface Characteristics and Enhanced in Vivo Osseointegration of Alkali-Treated Titanium with Nanonetwork Structures. *Int. J. Mol. Sci.* **2019**, *20*, 1127. [[CrossRef](#)] [[PubMed](#)]
22. Engel, E.; Michiardi, A.; Navarro, M.; Lacroix, D.; Planell, J.A. Nanotechnology in regenerative medicine: The materials side. *Trends Biotechnol.* **2008**, *26*, 39–47. [[CrossRef](#)] [[PubMed](#)]
23. Cai, K.Y.; Bossert, J.; Jandt, K.D. Does the nanometre scale topography of titanium influence protein adsorption and cell proliferation? *Colloid Surf. B-Biointerfaces* **2006**, *49*, 136–144. [[CrossRef](#)] [[PubMed](#)]
24. Webster, T.J.; Schadler, L.S.; Siegel, R.W.; Bizios, R. Mechanisms of enhanced osteoblast adhesion on nanophase alumina involve vitronectin. *Tissue Eng.* **2001**, *7*, 291–301. [[CrossRef](#)] [[PubMed](#)]
25. Kim, C.; Kendall, M.R.; Miller, M.A.; Long, C.L.; Larson, P.R.; Humphrey, M.B.; Madden, A.S.; Tas, A.C. Comparison of titanium soaked in 5 M NaOH or 5 M KOH solutions. *Mater. Sci. Eng. C* **2013**, *33*, 327–339. [[CrossRef](#)] [[PubMed](#)]
26. Tang, P.; Jiang, S.; Wang, G. Research Progress of Surface Modification Coatings on Titanium Alloys for Bone Implants. *Mater. China* **2021**, *40*, 631–638.
27. Schwarz, F.; Wieland, M.; Schwartz, Z.; Zhao, G.; Rupp, F.; Geis-Gerstorfer, J.; Schedle, A.; Broggini, N.; Bornstein, M.M.; Buser, D.; et al. Potential of Chemically Modified Hydrophilic Surface Characteristics to Support Tissue Integration of Titanium Dental Implants. *J. Biomed. Mater. Res. B* **2009**, *88B*, 544–557. [[CrossRef](#)]
28. Zhang, L.C.; Chen, L.Y.; Wang, L.Q. Surface Modification of Titanium and Titanium Alloys: Technologies, Developments, and Future Interests. *Adv. Eng. Mater.* **2020**, *22*, 1901258. [[CrossRef](#)]
29. Wang, F.; Zhang, S.; Shu, J.; Gao, Y.; Sun, X.; Wang, Q. Effects of surface modification of titanium implants on the osseointegration. *Chin. J. Tissue Eng. Res.* **2014**, *18*, 8491–8497.
30. Hou, C.; An, J.; Zhao, D.Y.; Ma, X.; Zhang, W.L.; Zhao, W.; Wu, M.; Zhang, Z.Y.; Yuan, F.S. Surface Modification Techniques to Produce Micro/Nano-scale Topographies on Ti-Based Implant Surfaces for Improved Osseointegration. *Front. Bioeng. Biotechnol.* **2022**, *10*, 835008. [[CrossRef](#)]
31. Yan, X.X.; Cao, W.; Li, H.H. Biomedical Alloys and Physical Surface Modifications: A Mini-Review. *Materials* **2022**, *15*, 66. [[CrossRef](#)] [[PubMed](#)]
32. Yang, B.-C.; Zhou, X.-D.; Yu, H.-Y.; Wu, Y.; Bao, C.-Y.; Man, Y.; Cheng, L.; Sun, Y. Advances in titanium dental implant surface modification. *West China J. Stomatol.* **2019**, *37*, 124–129. [[CrossRef](#)]
33. Shen, H.; You, D.; Zhang, P.; Li, W. Preparation of Porous Titanium with NH₄HCO₃ as a Space Holder by Powder Metallurgy and Its Mechanical Properties. *Spec. Cast. Nonferr. Alloy.* **2016**, *36*, 291–294.
34. Wang, Y.Q.; Tao, J.; Zhang, J.L.; Wang, T. Effects of addition of NH₄HCO₃ on pore characteristics and compressive properties of porous Ti-10%Mg composites. *Trans. Nonferr. Met. Soc. China* **2011**, *21*, 1074–1079. [[CrossRef](#)]
35. Liu, X.M.; Wu, S.L.; Yeung, K.W.K.; Xu, Z.S.; Chung, C.Y.; Chu, P.K. Superelastic Porous NiTi with Adjustable Porosities Synthesized by Powder Metallurgical Method. *J. Mater. Eng. Perform.* **2012**, *21*, 2553–2558. [[CrossRef](#)]
36. Alves, A.C.; Costa, A.I.; Toptan, F.; Alves, J.L.; Leonor, I.; Ribeiro, E.; Reis, R.L.; Pinto, A.M.P.; Fernandes, J.C.S. Effect of bio-functional MAO layers on the electrochemical behaviour of highly porous Ti. *Surf. Coat. Technol.* **2020**, *386*, 125487. [[CrossRef](#)]
37. Ho, W.F.; Lai, C.H.; Hsu, H.C.; Wu, S.C. Surface modification of a low-modulus Ti-7.5Mo alloy treated with aqueous NaOH. *Surf. Coat. Technol.* **2009**, *203*, 3142–3150. [[CrossRef](#)]
38. Lu, M.X.; Chen, H.J.; Yuan, B.; Zhou, Y.; Min, L.; Xiao, Z.W.; Yang, X.; Zhu, X.D.; Tu, C.Q.; Zhang, X.D. The morphological effect of nanostructured hydroxyapatite coatings on the osteoinduction and osteogenic capacity of porous titanium. *Nanoscale* **2020**, *12*, 24085–24099. [[CrossRef](#)] [[PubMed](#)]

39. Chen, X.; Zhu, R.F.; Gao, H.; Xu, W.L.; Xiao, G.Y.; Chen, C.Z.; Lu, Y.P. A high bioactive alkali-treated titanium surface induced by induction heat treatment. *Surf. Coat. Technol.* **2020**, *385*, 125362. [[CrossRef](#)]
40. Chen, X.B.; Li, Y.C.; Hodgson, P.D.; Wen, C. The importance of particle size in porous titanium and nonporous counterparts for surface energy and its impact on apatite formation. *Acta Biomater.* **2009**, *5*, 2290–2302. [[CrossRef](#)]
41. Li, J.S.; Wang, X.H.; Hu, R.; Kou, H.C. Structure, composition and morphology of bioactive titanate layer on porous titanium surfaces. *Appl. Surf. Sci.* **2014**, *308*, 1–9. [[CrossRef](#)]
42. Ye, Q.; He, G. In-situ formed graded microporous structure in titanium alloys and its effect on the mechanical properties. *Mater. Des.* **2015**, *83*, 295–300. [[CrossRef](#)]
43. Wang, X.H.; Li, J.S.; Hu, R.; Kou, H.C. Mechanical properties and pore structure deformation behaviour of biomedical porous titanium. *Trans. Nonferr. Met. Soc. China* **2015**, *25*, 1543–1550. [[CrossRef](#)]
44. Yuan, L.; Ding, S.L.; Wen, C.E. Additive manufacturing technology for porous metal implant applications and triple minimal surface structures: A review. *Bioact. Mater.* **2019**, *4*, 56–70. [[CrossRef](#)] [[PubMed](#)]
45. Zhao, X.C.; Ren, X.J.; Wang, C.Z.; Huang, B.X.; Ma, J.; Ge, B.; Jia, Z.F.; Li, Y.C. Enhancement of hydroxyapatite formation on titanium surface by alkali heat treatment combined with induction heating and acid etching. *Surf. Coat. Technol.* **2020**, *399*, 126173. [[CrossRef](#)]